9700 *Inorg. Chem.* **2009**, *48*, 9700–9714
DOI: 10.1021/ic901054h

Inorganic Chemistry
Article

Solvation Effects on Isomeric Preferences of Curium(III) Complexes with Multidentate phosphonopropionic Acid Ligands: CmH_2PPA^{2+} and $CmHPPA^{+}$ Complexes

Zhiji Cao,[†] K. Balasubramanian,*[,†,‡,§] Michael G. Calvert,[§,∥] and Heino Nitsche[§,∥]

[†]*College of Science, California State University, East Bay, Hayward, California 94542,* [‡]*Chemistry and Material Science Directorate Lawrence Livermore National Laboratory Livermore, California 94550,* [§]*Nuclear Science Division, Lawrence Berkeley National Laboratory, Berkeley, California 94720, and* [∥]*Department of Chemistry, University of California, Berkeley, California 94720*

Received June 1, 2009

We have carried out both time-resolved laser fluorescence spectroscopic and computational studies on the complexes of curium(III) with multidentate Phosphonopropionic (PPA) acid ligands. A number of complexes of Cm(III) with these ligands, such as CmH_2PPA^{2+}, $CmHPPA^{+}$, $Cm[H_2PPA]_2^{+}$, and $Cm[HPPA]_2^{-}$ have been studied. Our computational studies focused on all possible isomers in the gas phase and aqueous solution so that the relative binding strengths of carboxylic versus phosphoric groups can be assessed in these multidentate systems. The solvation effects play an important role in the determination of the preferred configurations and binding propensities of carboxylate versus phosphate sites of the ligands. Our computations assess the relative strengths of single and multidentate complexes in solutions for these systems. The computed free energies of solvation explain the experimentally observed fluorescence spectra and the lifetimes of these complexes in that as more water molecules are displaced from the first hydration sphere by the ligands that bind to Cm(III), the fluorescence lifetime increases. We have found that the most stable complex for CmH_2PPA^{2+} in the aqueous phase exhibits a monodentate complex where the curium(III) is bound to the deprotonated phosphate oxygen atom. Our computations support the observed longer fluorescence lifetime of CmH_2PPA^{2+} (112 μs) compared to the free Cm(III) aquo ion (65 μs), suggesting a greater degree of H_2O displacement from the hydration sphere. For the Cm-$HPPA^{+}$ complex, we find a tridentate form as the most stable structure which supports the observed fluorescence lifetime for the $CmHPPA^{+}$ complex (172 μs), confirming the removal of up to six water molecules from the inner hydration sphere. The relative stabilities of the complexes are found to vary substantially between the gas phase and solution, indicating a major role of solvation in the relative stabilities of these complexes.

1. Introduction

Actinide coordination chemistry and spectroscopy have been the topics of a number of experimental studies,[1−26] as actinides exhibit interesting coordination chemistry and bondings because of the intriguing roles of the 5f and 6d orbitals. Actinide complexes have also drawn increased attention in recent years because of increased nuclear activity that produces high-level nuclear wastes. Chemical bonding

*To whom correspondence should be addressed. E-mail: balu@llnl.gov.

(1) Clark, D. L.; Hobart, D. E.; Neu, M. P. *Chem. Rev.* **1995**, *95*, 25.
(2) Lombardi, J. R.; Davis, B. *Chem. Rev.* **2002**, *102*, 2431.
(3) Szabo, Z.; Toraishi, T.; Vallet, V.; Grenthe, I. *Coord. Chem. Rev.* **2006**, *250*, 784.
(4) Clark, D. L.; Conradson, S. D.; Keogh, D. W.; Palmer, P. D.; Scott, B. L.; Tait, C. D. *Inorg. Chem.* **1998**, *37*, 2893.
(5) Valle, A.; Chinea, E.; Dominguez, S.; Mederos, A.; Midollini, S.; Vacca, A. *Polyhedron* **1999**, *18*, 3253.
(6) Beveridge, T. J. *Annu. Rev. Microbiol.* **1989**, *43*, 147.
(7) Kim, J. I.; Freeman, A. J.; Keller, C. *Handbook of the Chemistry and Physics of Actinides*; Elsevier: Amsterdam, 1986; Vol. *4*.
(8) Kimura, T.; Choppin, G. R. *J. Alloys Compd.* **1994**, *213*, 313.
(9) Kimura, T.; Choppin, G. R.; Kato, Y.; Yoshida, Z. *Radiochim. Acta* **1996**, *72*, 61.
(10) Nitsche, H.; Silva, R. J. *Radiochim. Acta* **1996**, *72*, 65.
(11) Allen, P. G.; Bucher, J. J.; Clark, D. L.; Edelstein, N. M.; Ekberg, S. A.; Gohdes, J. W.; Hudson, E. A.; Kaltsoyannis, N.; Lukens, W. W.; Neu, M. P.; Palmer, P. D.; Reich, T.; Shuh, D. K.; Tait, C. D.; Zwick, B. D. *Inorg. Chem.* **1995**, *34*, 4797.
(12) Panak, P. J.; Nitsche, H. *Radiochim. Acta* **2001**, *89*, 499.
(13) Moll, H.; Stumpf, T.; Merroun, M.; Rossberg, A.; Selenska-Pobell, S.; Bernhard, G. *Environ. Sci. Technol.* **2004**, *38*, 1455.
(14) Barkleit, A.; Moll, H.; Bernhard, G. *Dalton Trans.* **2008**, 2879.
(15) Klenze, R.; Panak, P.; Kim, J. I. *J. Alloys Compd.* **1998**, *271*, 746.
(16) Wimmer, H.; Klenze, R.; Kim, J. I. *Radiochim. Acta* **1992**, *56*, 79.
(17) Cavellec, R.; Lucas, C.; Simoni, E.; Hubert, S.; Edelstein, N. *Radiochim. Acta* **1998**, *82*, 221.
(18) Moll, H.; Geipel, G.; Bernhard, G. *Inorg. Chim. Acta* **2005**, *358*, 2275.
(19) Fanghanel, T.; Kim, J. I.; Paviet, P.; Klenze, R.; Hauser, W. *Radiochim. Acta* **1994**, *66*−*7*, 81.
(20) Wang, Z. M.; Felmy, A. R.; Xia, Y. X.; Buck, E. C. *J. Alloys Compd.* **2006**, *418*, 166.
(21) Brandt, H.; Bosbach, D.; Panak, P. J.; Fanghanel, T. *Geochim. Cosmochim. Acta* **2007**, *71*, 145.
(22) Panak, P. J.; Kim, M. A.; Klenze, R.; Kim, J. I.; Fanghanel, T. *Radiochim. Acta* **2005**, *93*, 133.
(23) Pathak, P. N.; Choppin, G. R. *Radiochim. Acta* **2007**, *95*, 137.

 Published on Web 09/17/2009

and migration of actinides in high-level nuclear waste in both geological and biological environments has been of prime concern over the years. Actinide ions present in these high-level wastes seem to exhibit complex equilibria of solvation in groundwater, and sorption onto minerals and bacteria or migration by binding into mobile particles such as colloidal silica. Consequently, it is important to understand the mechanisms and the nature of various processes that govern actinide migration and sorption. Curium(III) is found among nuclear waste products, as it is one of the byproducts of nuclear fission reactions. Among the nuclear fission products found in these wastes, Cm(III) exhibits high fluorescence spectroscopic sensitivity, and thus Cm(III) has attracted considerable experimental interest pertaining to its coordination chemistry and complexes of Cm(III).[13−26] A number of spectroscopic and other experimental studies have been carried out on microbial and environmental complexes of Cm(III) as well as other actinides.[12−26] Time-resolved laser fluorescence spectroscopy (TRLFS) has proven to be a promising tool for investigating the complexes formed by actinides in both geochemical and biochemical environments.[16−26] Panak and Nitsche[12] have demonstrated the use of TRLFS for the complexes of actinides with the *Bacillus sphaericus* strain. The spectra obtained for actinides with this strain exhibit considerable similarity to the spectra of organic and inorganic phosphates, suggesting the importance of actinide-phosphate complexes as adenosine phosphates groups in the bacteria seem to be the primary binding ligands in these complexes. Moll et al.[18] have shown that the TRLFS method is useful in studying Cm(III) complexes with ATP. Wimmer et al.[16] have studied the hydrolysis of Cm(III) reactions by TRLFS, while Cavellec et al.[17] have shown that structural characterization of sorption complexes of Cm(III) at the phosphate minerals-solution interface is feasible by the use of laser spectrofluorimetry. Valle et al.[5] have proposed that Be(II) complexes form 7-membered rings with phosphonopropionic acids which seem to serve as models for further validation in our current studies on Cm(III) complexes. Calvert et al.[24−26] have investigated the TRLFS spectra of Eu(III) and Cm(III) complexes with phosphonoacetic, phosphonopropionic acids, and EDTA.

We have chosen to investigate phosphonoacetic (PAA) and phosphonopropionic acids (PPA) complexes with Cm(III), as part of a model system for studying the multifunctionality of a bacterial surface. Both ligands have a phosphate group ($-OPO_3H_2$) and a carboxylate group ($-COOH$) on the two ends of an alkyl chain. These groups, as well as their proximity to each other, may work in concert the way reactive groups on a bacterial surface might. Both PAA and PPA have individual acid dissociation constants that are separated from each other by several pH units. For example, because of the lower pK_a, phosphate groups generally deprotonate at a much lower pH than carboxylate groups, thus making it possible to study their actinide binding individually even when carboxylate groups are present on the same molecule. As the pH increases and approaches the pK_a value for carboxylate deprotonation (4.5−5.0), it is likely that the nature of the complex changes, and the carboxylate group will begin to deprotonate and participate in the complex formation. The bidentate nature of the metal−ligand interaction can produce a highly stabilized complex. To study if this complex is competitive or synergistic between the phosphate and the carboxylate groups, both experimental results and theoretical calculations are presented here.

A number of theoretical studies have focused on the coordination chemistry and nature of bonding of actinides.[27−40] Among the actinides, curium is particularly interesting as it lies at the center of the actinide series with a half-filled 5f shell and a 6d shell containing a single electron. Thus the relative role played by 5f versus 6d orbitals is particularly interesting in actinide complexes. The 6d orbitals of early actinides are lower in energies and thus exhibit greater participation in bonding while the latter members of the series do not, and thus Cm would be an interesting candidate as it falls right in the middle of actinide series. Moreover, relativistic effects are known to be important for such heavy atom containing species[40] which could have a strong influence on the nature of bonding and the coordination chemistry of Cm(III) complexes. The other fundamentally interesting question pertains to the coordination of Cm(III) in aqueous solution and how that plays a role in the fluorescence lifetimes. Cm(III) is especially interesting in this regard as it exhibits up to 9-fold water coordination.[8] The lifetimes of these complexes have exhibited strong dependence on the number of water molecules bound to Cm(III) in the first hydration sphere.[8]

Stimulated by these interesting spectroscopy and fundamental coordination chemistry-concerning Cm-complexes, we have carried out spectroscopic and computational studies on Cm(III) with multidentate phosphonopropionic acids (PPA) ligands in solution. We have carried out relativistic computational studies and TRLFS studies to investigate the nature of the most stable complexes in solution and how the fluorescence lifetimes correlate with the coordination chemistry of these complexes.

2. Materials and Methods

2.1. Computational Methods. We have optimized the equilibrium geometries of a number of Cm(III) complexes considering

(24) Calvert, M. G.; *Curium(III) and Europium(III) Complexation with Multifunctional Ligands Investigated by Time-Resolved Laser Fluorescence Spectroscopy*. Ph.D. Thesis, University of California, Berkeley, Department of Chemistry, May **2009**.

(25) Calvert, M. G.; Oyama Hui, A.; Nitsche, H. Multifunctional Polyelectrolytes as Model Compounds for Humic Acids and Surfaces of Soil Bacteria: Cm(III)/Eu(III) binding investigated by TRLFS. *Radiochim. Acta* **2009**, to be submitted.

(26) Calvert, M. G.; Oyama Hui, A.; Nitsche, H. Multifunctional Polyelectrolytes as Model Compounds for Humic Acids and Surfaces of Soil Bacteria: pK_a values, manuscript in preparation.

(27) Schreckenbach, G.; Hay, P. J.; Martin, R. L. *Inorg. Chem.* **1998**, *37*, 4442.

(28) Schreckenbach, G.; Hay, P. J.; Martin, R. L. *J. Comput. Chem.* **1999**, *20*, 70.

(29) Hay, P. J.; Martin, R. L.; Schreckenbach, G. *J. Phys. Chem. A* **2000**, *104*, 6259.

(30) Tuan, D. F. T.; Pitzer, R. M. *J. Phys. Chem.* **1996**, *100*, 6277.

(31) Zhang, Z. Y.; Pitzer, R. M. *J. Phys. Chem. A* **1999**, *103*, 6880.

(32) Matsika, S.; Pitzer, R. M. *J. Phys. Chem. A* **2000**, *104*, 4064.

(33) Matsika, S.; Pitzer, R. M. *J. Phys. Chem. A* **2001**, *105*, 637.

(34) Matsika, S.; Zhang, Z.; Brozell, S. R.; Baudeau, J. P.; Wang, Q.; Pitzer, R. M. *J. Phys. Chem. A* **2001**, *105*, 3825.

(35) Sonnenberg, J. L.; Hay, P. J.; Martin, R. L.; Bursten, B. E. *Inorg. Chem.* **2005**, *44*, 2255.

(36) Cao, Z. J.; Balasubramanian, K. *J. Chem. Phys.* **2005**, 123.

(37) Majumdar, D.; Balasubramanian, K.; Nitsche, H. *Chem. Phys. Lett.* **2002**, *361*, 143.

(38) Wheaton, V.; Majumdar, D.; Balasubramanian, K.; Chauffe, L.; Allen, P. G. *Chem. Phys. Lett.* **2003**, *371*, 349.

(39) Chaudhuri, D.; Balasubramanian, K. *Chem. Phys. Lett.* **2004**, *399*, 67.

(40) Balasubramanian, K. *Relativistic Effects in Chemistry Part A and B*; Wiley-Interscience: New York, 1997.

multidentate features of the ligands considered here both in the gas phase and in aqueous solution. We have uniformly computed the vibrational frequencies and IR spectra to ensure that the computed optimized geometries are true minima. All of the computations were carried out using the density functional theory (DFT) approach in conjunction with the relativistic effective core potentials (RECPs) for Cm(III) and the B3LYP functionals.[41−44] The effect of the solvent (water) was studied using self-consistent reaction field (SCRF) models by treating the solvent to be a dielectric continuum within the integral equation formalism polarized continuum model (IEFPCM). The geometries were fully optimized without symmetry restrictions using these models to seek their structures in the aqueous medium. We have also explicitly included water molecules that are quantum mechanically bound if the ligands do not saturate the coordination number. In the IEFPCM model, the solute is immersed in a shape-adapted cavity defined by interlocking spheres centered on each solute atom or group and with standard UATM (United Atomic Topological Model) radii.

All the calculations were carried out using RECPs which replace the 78 core electrons of curium.[45] The valence 6s, 6p, 5f, 6d, and 7s electrons are explicitly treated using primitive Gaussian basis sets of [7s6p5d5f] quality for Cm. We have also utilized the Stuttgart basis set combined with a small core 60-electron RECPs[47,48] to compare our results obtained using the 78-electron core RECPs. Moreover the effect of 5g functions was also tested. Excellent agreement among the various techniques was obtained for the equilibrium geometries, although the energy separations of excited states tend to depend on the levels of theory. Moreover it is computationally prohibitive to use larger Stuttgart basis sets, especially in solution computations and the computation of free energies. Thus we have uniformly employed 78-electron core RECPs for Cm. We have also found the effect of 5g functions on these complexes to be negligible and thus these functions were not included for larger complexes in solution. For the carbon and oxygen atom, RECPs were employed retaining the outer 2s and 2p shells in the valence space, again choosing compatible valence Gaussian basis sets. The carbon and oxygen basis sets from Pacios and Christiansen[46] were augmented with sets of six component 3d Gaussian functions (α_d = 0.75 for carbon, and 0.85 for oxygen). For phosphorus, RECPs[46] were employed retaining the outer 3s and 3p shells in the valence space, and the corresponding basis set for the element was augmented with six component 3d Gaussian functions (α_{d1} = 1.2 and α_{d2} = 0.3). The Van Duijneveldt's[49] hydrogen basis set was used for the hydrogen atoms augmented by a set of 2p polarization functions.

We have also recently carried out relativistic CASSCF/MRSDCI and RCI computations including spin−orbit effects on curium hydrides.[51] The results of these high-level computations clearly show that the ground states of curium species are predominantly single configurational and thus do not require MCSCF or CASSCF treatments, and electron correlation effects from the predominant configuration play the most important role in the characterization of the geometry and energetics of the ground states of these species. Moreover, the spin−orbit effects were found to clearly correlate to the atomic states of Cm or the ion depending on the complex in question. This is understandable as the 5f orbitals of the latter actinides in the series are core-like and do not bind strongly to the ligands and retain their open-shell characteristics. Thus the spin−orbit effects of Cm complexes can be predicted from the atomic states of Cm.

Scheme 1. Thermodynamic Cycle Considered for Calculating Solvation Free Energies in Aqueous Solution

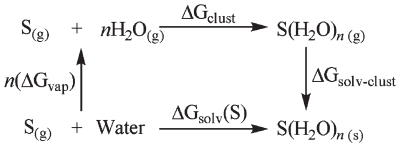

Scheme 2. Thermodynamic Cycle for the Calculation of the Reaction Gibbs Energies in Aqueous Solution

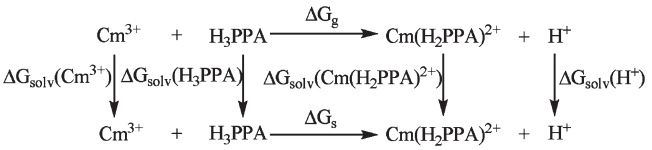

The discrete-continuum model has been applied to the calculations of the solvation free energies of ionic solutes from the thermodynamic cycle presented in Scheme 1. Thus solvation free energies are calculated as (S denotes the solute)

$$\Delta G_{\mathrm{solv}}(\mathrm{S}) = n\Delta G_{\mathrm{vap}} + \Delta G_{\mathrm{clust}} + \Delta G_{\mathrm{solv\text{-}clust}}$$

where $n\Delta G_{\mathrm{vap}}$ is the Gibbs free energy required to move n water molecules from the pure liquid phase to the gas phase to form the cluster with the solute, $\Delta G_{\mathrm{clust}}$ is the free energy of formation of the cluster $S(H_2O)_n$ in the standard state (1 mol/L), $\Delta G_{\mathrm{solv-clust}}$ is the solvation free energy of the cluster corresponding to the long-range interactions of the hydrated cluster embedded in a cavity, which refers to the process of gas (1 mol/L) → solution (1 mol/L).

The Gibbs energy of the reaction of $Cm^{3+} + H_3PPA \rightarrow CmH_2PPA^{2+} + H^+$ was computed from the thermodynamic cycle presented in Scheme 2. Thus, the reaction Gibbs energy in aqueous solution is calculated as

$$\Delta G_s = \Delta G_g + \Delta G_{\mathrm{solv}}(\mathrm{CmH_2PPA^{2+}}) + \Delta G_{\mathrm{solv}}(\mathrm{H^+}) - \Delta G_{\mathrm{solv}}(\mathrm{Cm^{3+}}) - \Delta G_{\mathrm{solv}}(\mathrm{H_3PPA})$$

where ΔG_{solv} is the solvation free energy.

All of the calculations were carried out using the GAUSSIAN 03 package of codes.[50]

2.2. Experimental Techniques. Preparation of ^{248}Cm(III) PAA and PPA Complexes. The ^{248}Cm ($t_{1/2} = 3.4 \times 10^5$ years) complexes considered here were made from a Cm source obtained from Oak Ridge National Laboratory, under REDC Shipment No. 1918. A stock solution was prepared by dissolving the curium metal in a solution of 1 M $HClO_4$ and was confirmed to be ^{248}Cm (97.3%), ^{246}Cm (2.62%), and ^{244}Cm (0.02%) by using a Wallac Liquid Scintillation Counter. 3-Phosphonopropionic acids (PPA) was obtained in reagent grade (99.999%) quantities from Alfa Aesar. All solutions were made from CO_2-free distilled water supplied from a Barnstead Still coupled to a Millipore Milli-Q purifying apparatus (resistivity > 18 MΩ). The ionic strength was adjusted to I = 0.05 M using $NaClO_4$ from Sigma-Aldrich (99.999%). The PAA and PPA systems were studied at various pH values in the range 1.5−6.5 under CO_2-free conditions 25 ± 0.2 C. The 3-phosphonopropionic acid (PPA) deprotonation constants were determined by high-precision, high-accuracy potentiometric

(41) Parr, R. G.; Yang, W. *Density Functional Theory of Atoms and Molecules*; Oxford: New York, 1989.
(42) Becke, A. D. *J. Chem. Phys.* **1993**, *98*, 5648.
(43) Vosko, S. H.; Wilk, L.; Nusair, M. *Can. J. Phys.* **1980**, *58*, 1200.
(44) Lee, C. T.; Yang, W. T.; Parr, R. G. *Phys. Rev. B* **1988**, *37*, 785.
(45) Nash, C. S.; Bursten, B. E.; Ermler, W. C. *J. Chem. Phys.* **1997**, *106*, 5133.
(46) Pacios, L. F.; Christiansen, P. A. *J. Chem. Phys.* **1985**, *82*, 2664.
(47) Cao, X. Y.; Dolg, M.; Stoll, H. *J. Chem. Phys.* **2003**, *118*, 487.
(48) Kuchle, W.; Dolg, M.; Stoll, H.; Preuss, H. *J. Chem. Phys.* **1994**, *100*, 7535.
(49) Duijneveldt, V. *IBM Tech. Res. Rep. RF1971*, 945.
(50) Frisch, M. J. et al. *Gaussian 03*, revision C.02; Gaussian, Inc.: Pittsburgh, PA, 2005.
(51) Balasubramanian, K.; Cao, Z. J. *Communicated* **2009**.

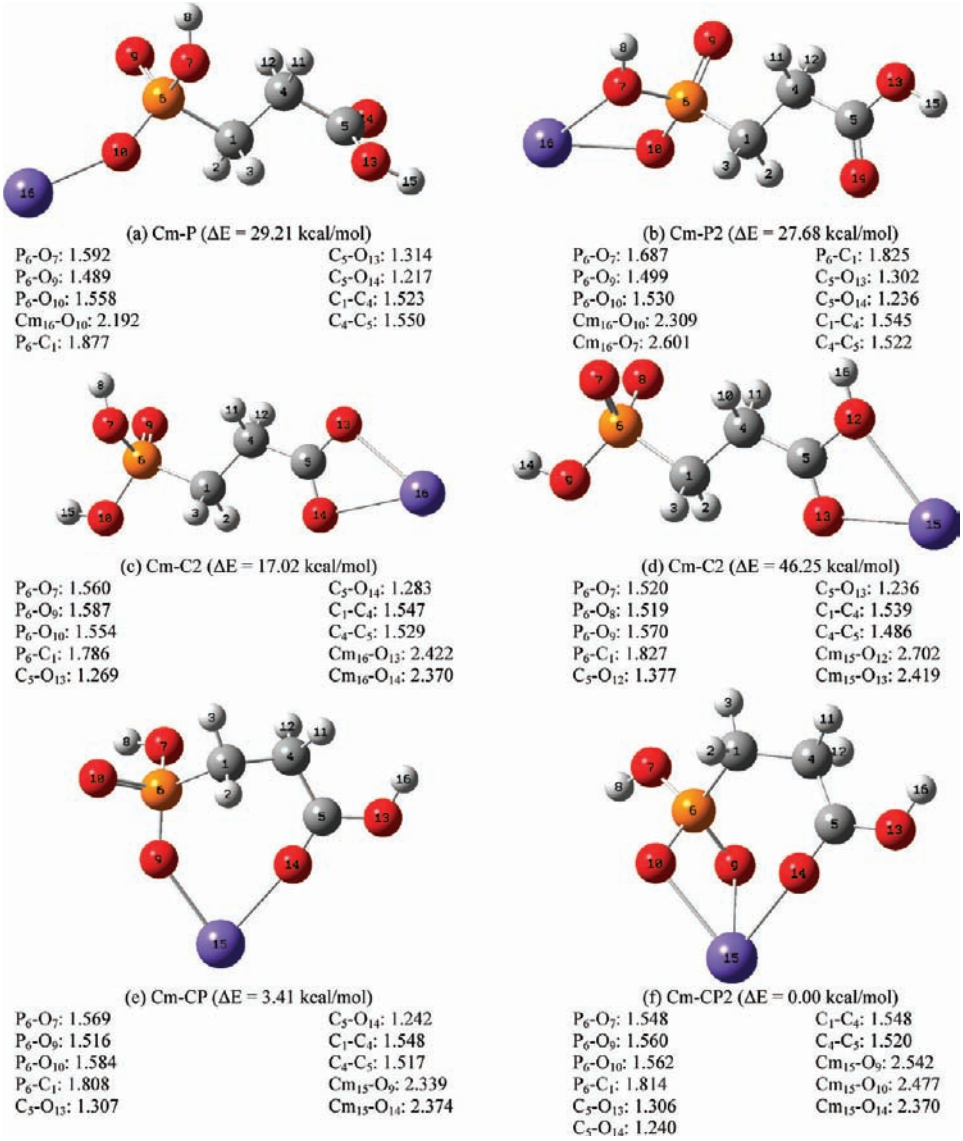

Figure 1. Optimized geometries (bond lengths in Å) of CmH_2PPA^{2+} in the gas phase.

titrations. Five hundred data points were collected for each titration curve, using volume additions of only 5μL for each titration step. The deprotonation constant values at infinite dilution are $pK_{a1} = 1.69 \pm 0.06$, $pK_{a2} = 4.91 \pm 0.04$, and $pK_{a3} = 8.19 \pm 0.08$.[24−26,28]

Laser Fluorescence Measurements. Our laser fluorescence measurements were made at 25 °C using a Nd:YAG Pro 250 laser with 5−10 ns pulse and 10 Hz frequency in line with a Spectra Physics Master Oscillator Power Oscillator (MOPO). The time gating was controlled by a Princeton Instruments ST-133 controller, which is a programmable timing generator (PTG). The software parameters varied for these experiments. We collected 1200 laser shots and constant time windows of 300 μs with an excitation wavelength of 396.5 nm being used for curium complexes. For time-dependent emission decay measurements, the delay time between laser pulse and exposure was varied by 5 μs for curium(III). The TRLFS spectra were measured after a sample equilibration time of 0.5−1 h. The peak intensities were correlated with the calibration curve of standards verified for curium concentration by liquid scintillation counting. The fluorescence emissions were passed through a 1200 lines mm^{-1} grating for the curium measurements to accommodate the various emissions. Spectra were recorded with the PI-Max CCD Camera, which contained a 1024 × 256 nm CCD array. The computer program WINSPEC 32 from Princeton Instruments was used for data collection. Spectra were calibrated with a neon lamp. Power was measured in real time by a Coherent Fieldmax II Thermo-Optical-Pyroelectric sensor. The deconvolution of background-subtracted spectra was carried out with PEAKFIT (v 4.0), and the spectra were fitted to Voigt functions.[24−27]

3. Results and Discussion

3.1. CmH_2PPA^{2+}. TRLFS measurements were obtained for the Cm-PPA complexes. The Cm(III) aquo ion is characterized by a fluorescence emission band maximum at 593.8 nm. There is a pronounced red shift of the emission as a result of complex formation with the PPA accompanied by an increase in the fluorescence emission lifetime from 65 μs for the Cm(III) aquo ion. The TRLFS spectra clearly support complexation between Cm(III) and PPA species, where PPA by way of binding to Cm(III) displaces water molecules in the first hydration sphere. An interesting feature of the PPA molecule is that it can bind to Cm(III) with the oxygen atoms of the phosphate group or the carboxylate group. Thus, relative binding strengths of these two ligands can

Table 1. Optimized Bond Distances R(Cm−O) (in Å) between Cm and Phosphate/Carboxylate Oxygen Atoms and Energy Differences ΔE (in kcal/mol) at the DFT/B3LYP Level

				ΔE (gas)	
system	R(Cm−O) (gas)	R(Cm−O) (IEFPCM)[a]	R(Cm−O) (DC)[b]	78 *e* RECP[c]	60 *e* RECP[d]
Cm-P	2.192	2.331	2.366	29.21	44.66
Cm-P2	2.309, 2.601			27.68	42.46
Cm-C		2.582	2.530		
Cm-C2	2.422, 2.370	2.637, 2.498		17.02	32.86
Cm-CP	2.339, 2.374	2.340, 2.572	2.325, 2.543	3.41	17.02
Cm-CP2	2.542, 2.477, 2.370	2.598, 2.499, 2.480	2.558, 2.529, 2.421	0.00	0.00

[a] The effect of the solvent (water) was studied using the SCRF models considering the solvent to be a dielectric continuum. Integral equation formalism PCM model (IEFPCM) was used for this purpose. [b] The mixed discrete-continuum model, where the first solvation shell is explicitly included in the solute definition. [c] RECPs replace the 78 core electrons of curium. The valence 6s, 6p, 5f, 6d, and 7s electrons are explicitly treated using Gaussian basis sets, i.e. [5s6p4d3f] for Cm. [d] The Stuttgart basis set and the 60-electron RECP for Cm.

play important roles in the nature and structure of the resulting complexes. To assess the nature of the binding propensities of these two groups, we have performed a series of computations of different Cm(III) complexes with various ligands considered here.

We have performed geometry optimizations of curium complexes of PPA in both the solution and the gas phases to obtain the minimum energy structure. We have obtained six different structures in the gas phase that are shown in Figure 1, where we have contrasted these structures with labels such as Cm-P, Cm-P2, Cm-C2, Cm-CP, Cm-CP2 depending on whether the phosphate group is involved in the complex formation by itself (Cm-P) or both phosphate and carboxylic groups are involved in a concerted manner (Cm-CP$_n$). We have compared in Table 1 the optimized geometries and relative energy separations both in the gas phase and in the solution for different Cm(III) complexes with H_2PPA^{2+}. As can be seen in Table 1, the calculated energy difference of the CmH_2PPA^{2+} complex indicates that the most stable structure in the gas phase is a tridentate complex that we designate as CM-CP2 (Figure 1f) where the Cm(III) ion is bound to two of the phosphate oxygen atoms and one carboxylate oxygen atom of the PPA ligand and hence the label Cm-CP2 in Figure 1f and Table 1 for this complex. The second most stable structure is a bidentate complex that we label Cm-CP (Figure 1e), as this involves complexation with an oxygen from each of the phosphate and carboxylate groups. As can be seen from Table 1, this complex is nearly degenerate with the tridentate Cm-CP2 (Figure 1f) complex in the gas phase in that it is only 3.4 kcal/mol higher in energy. As shown in Figure 1e, Cm is chelated by way of forming a 7-membered ring with H_2PPA^{2+}. The next stable structure that we found in the gas phase is a bidentate carboxylate complex that we designate as Cm-C2 (Figure 1c) which exhibits a 4-membered chelate ring composed of two oxygen atoms from the carboxylate group bound to Cm(III). The relative propensity of first deprotonation on the carboxylic acid group versus phosphate group in the formation of the bidentate complex requires some discussion. As can be seen from Figure 1, the bidentate carboxylate complex formed through deprotonation on the phosphate group (Cm-C2, Figure 1d) is 29.23 kcal/mol higher in energy than that of the complex shown in Figure 1c, where deprotonation occurs on the carboxylate group. Moreover, the monodentate carboxylate complex was not formed at all in the gas phase. All attempts to optimize the geometry of the monodentate carboxylate complex in the gas phase results in a more stable bidentate carboxylate complex. Among the optimized structures considered in Figure 1, the least stable structure among different classes in the gas phase is the monodentate phosphate complex (Cm-P, Figure 1a). However, the bidentate phosphate complex (Cm-P2, Figure 1b) is merely 1.53 kcal/mol more stable than the monodentate Cm-P (Figure 1a).

Table 2. Calculated Solvation Gibbs Energies of CmH_2PPA^{2+} (in kcal/mol) Using the Combined Discrete-Continuum Model and the Pure Continuum Model

system	$n\Delta G_{vap}$	ΔG_{clust}	$\Delta G_{solv-clust}$	ΔG_{solv}[a]	ΔG_{solv}[b]	Figure
Cm^{3+}	13.32	−494.17	−397.92	−878.77	−890.24	
Cm-P	11.84	−146.44	−203.14	−337.74	−379.63	2a
Cm-C	11.84	−49.38	−259.30	−362.73	−405.94	2c
Cm-CP	10.36	−113.09	−202.12	−304.85	−326.15	2d
Cm-CP2	8.88	−108.77	−189.90	−289.79	−315.09	2e

[a] The discrete-continuum model has been applied to the calculations of the solvation free energies of ionic solutes from the thermodynamic cycle presented in Scheme 1. Thus solvation free energies are calculated as (S denotes the solute) $\Delta G_{solv}(S) = n\Delta G_{vap} + \Delta G_{clust} + \Delta G_{solv-clust}$, where $n\Delta G_{vap}$ is the Gibbs free energy required to move n water molecules from the pure liquid phase to the gas phase to form the cluster with the solute, ΔG_{clust} is the free energy of formation of the cluster $S(H_2O)_n$ in the standard state (1 mol/L), $\Delta G_{solv-clust}$ is the solvation free energy of the cluster corresponding to the long-range interactions of the hydrated cluster embedded in a cavity, which refers to the process of gas (1 mol/L) → solution (1 mol/L). [b] The pure continuum IEFPCM solvation model.

We have also considered different approaches to gauge the accuracy of our computations, basis sets, and RECPs. While considering these complexes in solution, we have also included as many water molecules as needed to fully saturate the first hydration sphere so that reliable solvation Gibbs free energies can be computed. In our prior works,[36] we have compared large-core RECPs that included 6s, 6p, 7s, 6d, and 5f shells in the valence space for Np with the corresponding Gaussian basis sets to small-core 60-electron RECP with the Stuttgart basis set for Np carbonate complexes. It is to be noted that the small-core RECPs provided results of comparable accuracy to more extensive computations carried out using the Stuttgart basis set and the 60-electron RECP for Np complexes. We also benchmarked the DFT results against the CCSD as well as CASSCF/MRSDCI results on smaller complexes and found that the results were quite consistent because these complexes are predominantly single configurational in the ground states. Moreover, the geometry optimization and frequency computations with larger Stuttgart

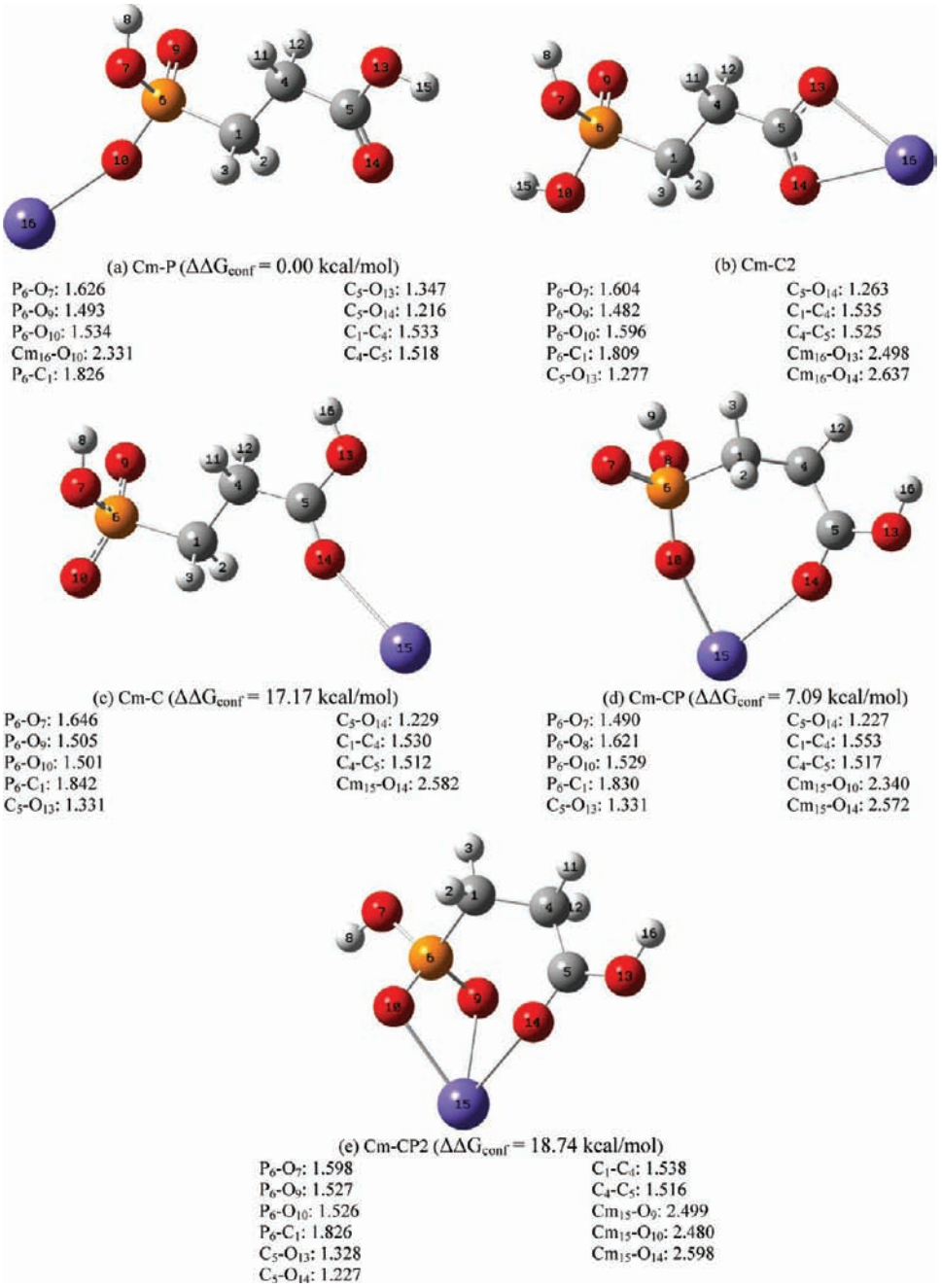

Figure 2. Optimized geometries (in Å) of CmH_2PPA^{2+} in pure continuum IEFPCM model.

basis sets are computationally quite intensive even at the DFT level. Thus, we conclude that the use of small core RECPs that include 6s, 6p, 7s, 5f, and 6d shells in the valence space is a more realistic approach for larger complexes. As can be seen in Table 1, the energy differences between the two methods have similar trends, except for the tridentate complex (Cm-CP2) which is more stable when 60-electron RECP was used. Thus the energy differences in the excited states between different basis sets for the same complex are between 13.61 and 15.84 kcal/mol. The geometries are much closer among different techniques although the energy differences of the excited states tend to be more sensitive to the levels of theory. However, these excited structures cannot be computed in solution by employing small-core ECPs and larger basis sets, as solvation Gibbs free energy thermodynamics computations require frequencies which are computationally quite expensive to compute. Thus, the large core RECPs with flexible basis sets provide more viable alternatives for free energy and vibrational frequency computations.

Solvation Gibbs energies have been obtained from the thermodynamic cycle presented in Scheme 1. The relevant data and the calculated solvation Gibbs energies are summarized in Table 2. The relative contributions of the various solvation terms to the three lowest structures are shown in Figure 6. The various continuum contributions ($\Delta G_{solv-clust}$) that depend on the size and shape of cavity do not change significantly, whereas the discrete contributions ($n\Delta G_{vap} + \Delta G_{clust}$) increase significantly

from the tridentate complex to monodentate phosphate complex because of the changes in the number of water molecules in the first hydration around the Cm^{3+}. This is expected in view of the fact that multidentate complexes would displace more water molecules from the first hydration sphere compared to monodentate complexes. This trend is clearly reflected in Figure 6 for the discrete contributions to the free energies indicating that the number of water molecules in the first hydration sphere plays a decisive role in solvation energies and stability in solution. Thus our results suggest that the specific solute−solvent interactions play a very important role in the conformational preference of CmH_2PPA^{2+} in aqueous solution. For the purpose of comparison, we have also computed solvation Gibbs energies using a pure continuum IEFPCM model without including water molecules in the first hydration sphere quantum chemically.

As can be seen in Table 2, the solvation Gibbs energies using the pure continuum model are generally larger than the values using the combined discrete-continuum model. The energy difference of between the Cm-P and Cm-C complexes is about 42 kcal/mol, whereas the corresponding energy difference is about 23 kcal/mol for Cm-CP and Cm-CP2 complexes. Consequently, it is critical to include all water molecules in the first hydration sphere explicitly in a quantum chemical treatment for the computation of Gibbs free energies. In a recent study[52] we have compared the solvation energies obtained by explicitly treating 20 water molecules that were in both the first and the second hydration spheres, and it was noted that it is not critical to include water molecules in the second hydration sphere quantum chemically for the computation of properties of the complex. Water molecules in the second and outer hydration spheres are best treated as a polarized continuum.

The optimized geometries and energy separations of CmH_2PPA^{2+} in aqueous solution for the various structures were computed using the IEFPCM continuum solvation model and the combined discrete-continuum model. The continuum solvent model elicits a relative stabilization of the CmH_2PPA^{2+} complex in aqueous solution. The equilibrium geometries in solution are presented in Figure 2. Their relative stabilization $\Delta\Delta G_{conf}$ in solution are also shown in Table 3. The conformational free energy difference (ΔG_{conf}) in solution was estimated by adding the solvation free energy $\Delta\Delta G_{sol}$ to the gas-phase energy, that is, $\Delta G_{conf} \approx \Delta E + \Delta\Delta G_{sol}$. As can be seen from Table 3, the calculations with the SCRF model, in contrast to those in the gas phase, give the most stable structure as the monodentate phosphate complex (Cm-P, Figure 2a) in aqueous solution, which in contrast is the least stable structure in the gas phase. This clearly demonstrates that it is imperative to study these complexes in aqueous solution rather than in the gas phase. As can be seen from Figure 2, we have also computed other viable low-lying structures such as a bidentate carboxylate complex (Cm-C2, Figure 2b), a CP2 bidentate complex (Cm-CP2, Figure 2e), and a bidentate Cm-CP complex (Figure 2d). The monodentate carboxylate complex, Cm-C, is found to exist as a higher energy structure in aqueous solution, although it is unstable in the gas phase. As can be seen from Table 3, although the tridentate complex is the most stable structure in the gas phase, it is 35.33 kcal/mol higher in solution than the monodentate phosphate complex.

Table 3. Relative Gas-Phase Energies, Gibbs Energies of Solvation, and Relative Conformational Gibbs Energies of CmH_2PPA^{2+} (in kcal/mol)

system	ΔE_g[a]	ΔG_{solv}[b]	$\Delta\Delta G_{conf}$[b]	$\Delta\Delta G_s$[c]	Figure
Cm-P	29.21	−379.63 (−337.74)	0.00 (0.00)	0.00	1a
Cm-C	71.37	−405.94 (−362.73)	15.85 (17.17)	18.82	2c
Cm-C2	17.02	−347.15	20.29		1c
Cm-CP	3.41	−326.15 (−304.85)	27.68 (7.09)		1e
Cm-CP2	0.00	−315.09 (−289.79)	35.33 (18.74)		1f
Cm-C2	46.25	−356.88	39.79		1d

[a] ΔE_g refers to gas-phase relative energy at the DFT/B3LYP level. [b] ΔG_{solv} and $\Delta\Delta G_{conf}$ refer to the Gibbs energy of solvation and the relative conformational Gibbs energy which was estimated by adding ΔG_{solv} to the gas-phase energy, using the pure continuum IEFPCM model and the combined discrete-continuum model (in parentheses). [c] The Gibbs energy of the reaction of $Cm^{3+} + H_3PPA \rightarrow CmH_2PPA^{2+} + H^+$ was computed from a thermodynamic cycle presented in Scheme 2. Thus, reaction Gibbs energy in aqueous solution is calculated as $\Delta G_s = \Delta G_g + \Delta G_{solv}(CmH_2PPA^{2+}) + \Delta G_{solv}(H^+) - \Delta G_{solv}(Cm^{3+}) - \Delta G_{solv}(H_3PPA)$, where ΔG_{solv} is the solvation free energy.

The dramatic differences in the relative stabilities between the gas-phase structures and aqueous solution structures arise because the bonding strength between the PPA group and Cm(III) is the primary driving force in the gas phase whereas the solvent−solute interactions are the primary driving force in solution. In the gas phase, the tridentate complex exhibits an enhanced bonding between the PPA and Cm(III), and thus it is the most stable structure. However, in aqueous solution the monodentate phosphate complex exhibits a greater degree of solvation effects at the carboxylate end. Thus, the most stable structure is the monodentate phosphate (Cm-CP) complex in aqueous solution.

The spin−orbit effects of curium need to be considered concerning the overall stability. In this regard we note that the ground state of the neutral Cm atom is Cm-($5f^7 7s^2 6d^1\ ^9D_2$). Evidently the ground state of Cm^+ is a $5f^7 7s^2\ ^8S_{7/2}$. Consequently, the Cm^{3+} ion involved in the complex has a $5f^7$ electronic configuration which gives rise to Cm^{3+} ($^8S_{7/2}$) ground state analogous to the ground state of Cm^+. The contribution of the 7s orbital to the spin−orbit effect is zero by definition and thus the spin−orbit effects on Cm^{3+} must be similar to those of Cm^+ and zero for the ground (S) states anyway. We have shown in a recent study[51] on CmH^+ that the net ground-state spin−orbit splitting is only 578 cm^{-1} although excited electronic states experience larger spin−orbit effects. Most importantly the spin−orbit stabilization to the total energy near the equilibrium geometry is nearly the same as at the dissociation limit as the $5f^7$ shell nearly retains its character at the molecular geometry and dissociation limit. Consequently, the spin−orbit effects cancel out in computing the dissociation energies and solvation energies relative to the dissociated species. On the basis of our extensive relativistic configuration interaction computations on curium species, we conclude that the spin−orbit contributions to the solvation energies for the ground states of the CmH_2PPA^{2+} and $CmHPPA^+$ complexes are less than 0.5 kcal/mol.

The nature of the bonding in the electronic states can be examined through charge populations obtained by a

(52) Cao, Z. J.; Balasubramanian, K. *Communicated* **2009**.

Table 4. Natural Population Analysis (Electrons) on Cm of CmH_2PPA^{2+} and Dipole Moment (D) in the Gas Phase and in Aqueous Solution

	gas phase					continuum IEFPCM model					discrete-continuum model				
		gross population					gross population					gross population			
system	atomic charge	5f	6d	7s	7p	atomic charge	5f	6d	7s	7p	atomic charge	5f	6d	7s	7p
Cm-P	1.89	8.02	0.06	0.02	0.01	2.93	7.03	0.03	0.01	0.01	2.52	7.12	0.08	0.24	0.01
Cm-C[a]						2.97	7.01	0.01	0.01		2.54	7.11	0.08	0.24	0.01
Cm-CP	1.91	8.01	0.05	0.03	0.01	2.91	7.04	0.03	0.02	0.01	2.51	7.14	0.09	0.23	0.01
Cm-CP2	1.93	7.97	0.05	0.05	0.01	2.84	7.08	0.04	0.03	0.01	2.49	7.16	0.08	0.23	0.01

[a] Cm-C is not a stable structure in the gas phase.

natural bond order analysis. Table 4 shows the computed charge populations for the various complexes considered here. The free Cm atom has an electronic charge of +3 prior to the complex formation but once the complex is formed the charge on Cm as well as individual orbital populations change. As can be seen from Table 4, the 5f orbital of Cm receives π back-donation from the oxygen atoms of phosphate and carboxylate, which results in a smaller partial charge of about 1.90 on Cm atom for the gas-phase CmH_2PPA^{2+} ion. The original population distribution on the 5f orbital is seven for Cm^{3+}. It changes to a value near eight for the complex in the gas phase after back-donation from oxygen atoms. The back-donations in Cm-CP and Cm-CP2 complexes are a little bit smaller. This might be due to the bending of the P−O−Cm and C−O−Cm moieties, which decreases the extent of π back-donation.

As can be seen in Table 4, the partial charges on the Cm atom vary dramatically between the gas phase and the aqueous solution. The charge of curium in solvated complexes is more positive in solution compared to the gas phase because of the polarization effects from the solvent which increase the positive charge by withdrawing electrons toward the solvent water molecules. The partial charge on the Cm atom is about 1.90, whereas it is about 2.90 in pure continuum model and about 2.50 in the combined discrete-continuum model, respectively. A pure continuum model overestimates the positive charge on Cm primarily because of the neglect of electron exchanges between the solute and its surrounding solvent molecules in the first hydration sphere. In any case, both solvation models predict significant charge transfers between the solute and the water molecules primarily in the first hydration sphere or the ligands bound directly to the Cm(III) ion. Compared to the population distribution in the pure continuum model, the 5f, 6d, and 7s orbitals have larger electron populations. The population analysis shows that the electronic charges on the curium ion are modified up to 0.4 from the pure continuum model to a cluster in the cavity. Therefore, the results show that the short-range interactions with water molecules in the first solvation shell are very strong and involve an appreciable amount of charge transfer, which is not predictable from bulk electrostatics. The bulk effects are also important and have significant effects on charge population distributions.

3.2. $CmHPPA^+$. We have obtained four different groups of stable structures for $CmHPPA^+$ in the gas phase, where $HPPA^{2-}$ refers the parent acid with a single proton in contrast to H_2PPA^- which has 2 protons. We have also optimized different structures in solution and have computed monodentate structures in solution which are not stable in the gas phase. Analogous to the diprotonated complexes, $CmHPPA^+$ forms tridentate (Figure 3f, Cm-CP2 in solution), bidentate mixed C−P (Figure 3e in solution), bidentate phosphate (Figure 3b in solution), and bidentate carboxylate (Figure 3d in solution) complexes. The gas-phase optimization of monodentate phosphate and monodentate carboxylate complexes results in Cm-P2 and Cm-C2 structures, respectively, indicating that monodentate complexes are not local minima in the gas phase. We have presented in Table 5 the relative energies of the various minima computed in the gas phase. As can be seen from Table 5, in the gas phase, the tridentate complex is the most stable structure, while the bidentate complex is 22.1 kcal/mol higher in energy. The energy difference between these two structures is much larger than that of 3.41 kcal/mol for the corresponding gas-phase structures of CmH_2PPA^{2+}. In contrast to CmH_2PPA^{2+}, the bidentate phosphate complex of $CmHPPA^+$ is more stable than the bidentate carboxylate complex. Whereas Cm-P2 is 10 kcal/mol lower in energy than Cm-C2 for $CmHPPA^+$, the corresponding Cm-P2 is 10 kcal/mol higher for CmH_2PPA^{2+}. We have also compared the computed energy differences at different levels using other techniques. We have employed the Stuttgart basis set and the corresponding 60-electron ECP for Cm and the results are compared with 78-electron RECPs in Table 5. Single point energies have been computed using the Stuttgart ECP and basis sets after optimizing the geometries using Gaussian basis sets and 78-electron RECP for Cm. As can be seen from Table 5, overall the results are comparable with the exception of the high lying Cm-C2 structure for which the difference in the energies is about 12 kcal/mol. The overall trend obtained by the use of the 78-electron RECP is the same as that of the Stuttgart basis set and corresponding 60-electron RECP. That is, all techniques predict the Cm-CP2 as the most stable isomer in the gas phase while the Cm-C2 structure is the least stable in the gas phase.

Figure 3 shows the optimized structures of $CmHPPA^+$ in aqueous solution. In aqueous solution, the Cm(III) ion is known to acquire a first hydration sphere composed of nine strongly bound water molecules. Consequently, we have explicitly included water molecules in the first hydration shell that are not displaced by the ligands. The remaining water molecules beyond the first hydration sphere were treated by the polarized continuum model. The optimized geometries of the hydrated $CmHPPA^+$ complex with H_2O molecules bound explicitly in the first hydration sphere to Cm(III) are shown in Figure 4. Table 5 compares the optimized bond distances R(Cm−O) both in phosphate/carboxylate groups for the gas phase and in aqueous solution. It can be seen from Table 5 that the change of

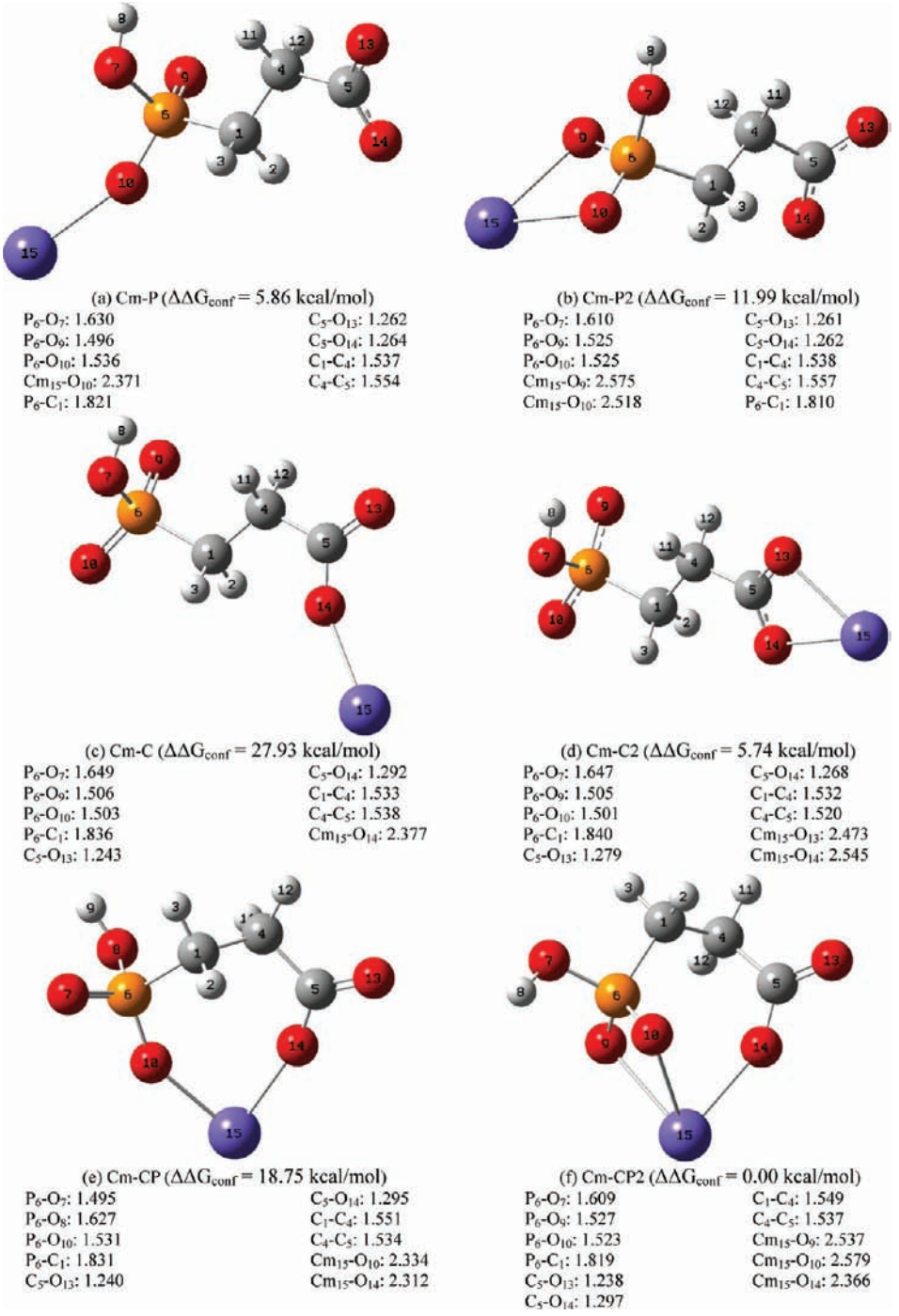

Figure 3. Optimized geometries (in Å) of $CmHPPA^+$ in aqueous solution.

structures owing to the solvent effect is significant. In aqueous solution, the monodentate phosphate complex (Cm-P, Figure 3a) and the monodentate carboxylate complex (Cm-C, Figure 3c) also exist as stable structures in addition to four other types of gas-phase structures. Compared to the gas-phase structures, the Cm−O bond distances in the continuum model are significantly elongated because of the solvent polarization effects. For example, the Cm−O bond distances of gas-phase Cm-C2 complex are 2.320 and 2.351 Å, whereas the corresponding values in the solution are 2.512 and 2.560 Å. For complexes in which water molecules in the first hydration sphere are explicitly included, the Cm−O bonds are still longer than those in the gas phase, but slightly shorter than those in a pure continuum model that did not include water molecules explicitly in the first hydration sphere. The Cm−O bond distances of Cm-C2 in the combined discrete-continuum model are 2.436 Å and 2.501 Å. In addition, it is interesting that the gas-phase bond distances between Cm and phosphate oxygen atom in Cm-CP and Cm-CP2 are shorter than the corresponding values for Cm and carboxylate oxygen atoms, although the trend is reversed in aqueous solution. This might be attributed to the differences in the solvation effects of phosphate and carboxylate groups.

Table 6 presents the Gibbs free energies of solvation and relative conformational Gibbs energies of $CmHPPA^+$. It

Table 5. Optimized Bond Distances R(Cm−O) (in Å) between Cm and Phosphate/Carboxylate Oxygen Atoms and Energy Differences ΔE (in kcal/mol) at the DFT/B3LYP Level

				ΔE (gas)	
system	R(Cm−O) (gas)	R(Cm−O) (IEFPCM)[a]	R(Cm−O) (DC)[b]	78 *e* RECP[c]	60 *e* RECP[d]
Cm-P		2.371	2.353		
Cm-P2	2.335, 2.348	2.518, 2.575	2.475, 2.482	23.17	29.37
Cm-C		2.377	2.440		
Cm-C2	2.320, 2.351	2.512, 2.560	2.436, 2.501	32.40	44.23
Cm-CP	2.217, 2.311(C)	2.334, 2.312(C)	2.329, 2.311(C)	22.08	25.21
Cm-CP2	2.385, 2.384, 2.449(C)	2.537, 2.579, 2.366(C)	2.516, 2.534, 2.369(C)	0.00	0.00

[a] The effect of solvent (water) was studied using the SCRF models considering the solvent to be a dielectric continuum. The integral equation formalism PCM model (IEFPCM) was used for this purpose. [b] The mixed discrete-continuum model, where the first solvation shell is explicitly included in the solute definition. [c] RECPs replace the 78 core electrons of curium. The valence 6s, 6p, 5f, 6d, and 7s electrons are explicitly treated using Gaussian basis sets, i.e. [5s6p4d3f] for Cm. [d] The Stuttgart basis set and the 60-electron RECP for Cm.

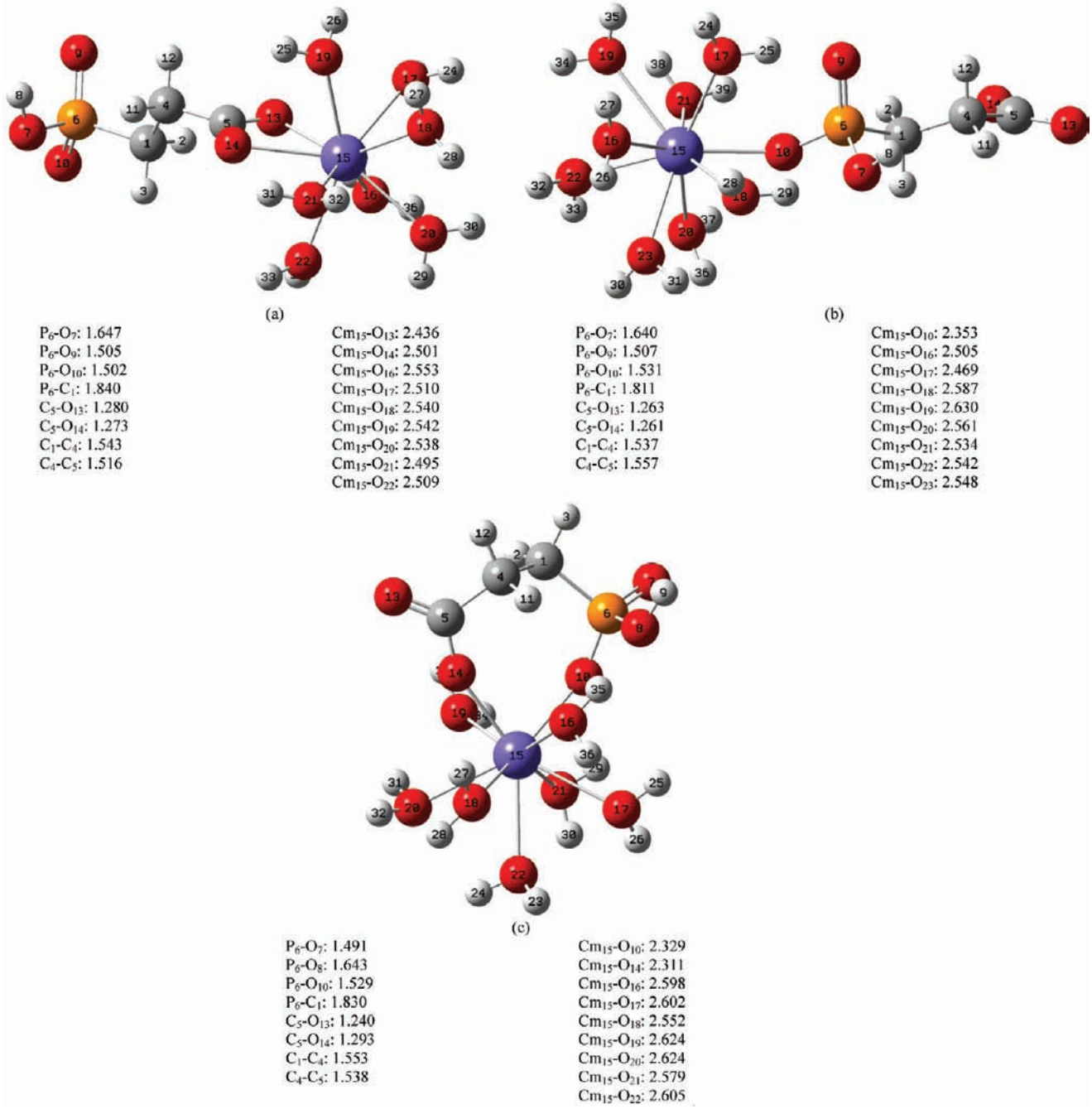

Figure 4. Optimized geometries (in Å) of $CmHPPA^{+}$ in aqueous solution with additional water molecules in the first solvation shell of Cm(III).

can be seen from Table 6 that ΔE_s, the relative energy differences among different structures are below 7 kcal/mol in the pure continuum model. The monodentate phosphate complex Cm-P and the bidentate complex Cm-CP are almost the same in energy in aqueous solution. The tridentate complex Cm-CP2 is only 3.05 kcal/mol higher in energy in the pure continuum model. Evidently, a pure continuum model is not adequate for the estimation of the relative solvation energies of nearly degenerate structures of charged species. This is because the cavity size is not well-defined in a pure continuum model, and moreover the solvent−solute interactions in the first hydration sphere are inherently quantum mechanical in nature and thus cannot be accurately represented by a continuum model. The mixed discrete-continuum model, where the first solvation shell is explicitly included in the solute definition, seems to be a more definitive way to study the geometries and energy separations of the various structures in solution. The inclusion of the first shell makes this model less dependent on the cavity size and shape selection. Compared to solvation Gibbs energies from the pure continuum model, the values computed using the combined discrete-continuum model are much smaller.

The determination of the conformational Gibbs energy in solution involves the calculation of solvation Gibbs energy and its algebraic addition to the gas-phase energy. As can be seen in Table 6, the ordering of different structures on the basis of the conformational Gibbs energies in solution is different from that of a pure continuum model. The Cm-CP2 tridentate complex of $CmHPPA^+$ is the most stable structure in aqueous solution followed by Cm-P and Cm-C2. The Cm-P and Cm-C structures are not stable in the gas phase. Aqueous solution geometries were used in the calculations of gas phase energies. As can be seen, the conformational Gibbs energy of Cm-P2 is only about 6 kcal/mol larger than that of Cm-C2. There results can be interpreted on the basis of the charge distributions (or polarization). Table 7 shows the natural population analysis both in gas phase and in aqueous solution. As can be seen from Table 7, analogous to CmH_2PPA^{2+}, the various computed structures of $CmHPPA^+$ exhibit dramatically increased 5f populations in the gas phase compared to the solution primarily because of the solvent polarization effects. There is a transfer of nearly one electron in the solution compared to the gas phase. This is consistent with increased positive charge on Cm in solution compared to the gas phase structures. As anticipated, most of the charge is received by the 5f orbitals of Cm.

Table 6. Relative Gas-Phase Energies, Gibbs Energies of Solvation and Relative Conformational Gibbs Energies of $CmHPPA^+$ (in kcal/mol)

system	ΔE_g[a]	ΔE_s[a]	ΔG_{solv}[b]	$\Delta\Delta G_{conf}$[b]	Figure
Cm-CP2	0.00	3.05	−154.89	0.00	3f
Cm-C2	32.40	4.34	−181.55	5.74	3d
Cm-P		0.63	−218.78	5.86	3a
Cm-P2	23.17	6.85	−166.07	11.99	3b
Cm-CP	22.08	0.00	−158.22	18.75	3e
Cm-C		2.64	−212.19	27.93	3c

[a] ΔE_g and ΔE_s refer to gas-phase relative energy and aqueous relative energy, respectively, computed using pure continuum IEFPCM model at the DFT/B3LYP level. [b] ΔG_{solv} and $\Delta\Delta G_{conf}$ refer to the Gibbs energy of solvation and the relative conformational Gibbs energy which was estimated by adding ΔG_{solv} to the gas-phase energy, using the combined discrete-continuum model.

3.3. $Cm(H_2PPA)_2^+$ and $Cm(HPPA)_2^-$. We have extended our computations to investigate the nature of complexes of Cm(III) with multiple H_2PPA^- and $HPPA^{2-}$ ligands. Figure 5 presents the optimized $Cm(H_2PPA)_2^+$ and $Cm(HPPA)_2^-$ complexes in aqueous solution. These structures have been confirmed to be local minima through vibrational frequency computations for the structures reported in Figure 5. As can be seen from Figure 6, both H_2PPA^- and $HPPA^{2-}$ form stable complexes with two of the ligands bound to Cm(III) in each case. In both structures both carboxylate and phosphate groups chelate to Cm(III) resulting in a six-coordinate complex shown in Figure 5. The remaining 3 coordination positions will be occupied by water molecules in the first hydration sphere. The computed Cm−O distances are comparable in the two complexes and the distances are generally shorter in the $Cm[H_2PPA]_2^+$ complex compared to the corresponding distances in $Cm[HPPA]_2^-$ in aqueous solution. This is expected in view of the two extra electrons in the anionic dimeric complex compared to the cationic complex. In the case of the $Cm[H_2PPA]_2^+$ complex the carboxylate oxygen distances are longer than the phosphate oxygen distances consistent with the enhanced binding strength of the phosphate group compared to the carboxylate group in H_2PPA^-. An opposite trend is observed in $Cm[HPPA]_2^-$ complex, as the parent ion $HPPA^{2-}$ is electron rich at the carboxylic oxygens. The optimized structures in solution thus show that the H_2PPA^- and $HPPA^{2-}$ ligands are multifaceted in not only binding through multiple sites on a given ligand but also multiple ligands can complex with Cm(III).

Figure 7 shows the relative contributions of the various solvation terms to four types of structures formed for $Cm[HPPA]^+$, especially for the lowest energy structures. In contrast to $Cm[H_2PPA]^{2+}$, both continuum contributions

Table 7. Natural Population Analysis (Electrons) on Cm of $CmHPPA^+$ and Dipole Moment (D) in the Gas Phase and in Aqueous Solution

	gas phase					continuum IEFPCM model					discrete-continuum model				
		gross population					gross population					gross population			
system	atomic charge	5f	6d	7s	7p	atomic charge	5f	6d	7s	7p	atomic charge	5f	6d	7s	7p
Cm-P[a]						2.94	7.02	0.02	0.01	0.01	2.52	7.12	0.08	0.24	0.01
Cm-P2	1.81	8.03	0.09	0.07	0.01	2.85	7.08	0.03	0.02	0.01	2.50	7.13	0.09	0.24	0.01
Cm-C[a]						2.93	7.03	0.03	0.01	0.01	2.49	7.14	0.09	0.24	0.01
Cm-C2	1.79	8.03	0.08	0.09	0.01	2.85	7.08	0.03	0.03		2.49	7.14	0.09	0.24	0.01
Cm-CP	1.86	8.00	0.08	0.06	0.01	2.84	7.08	0.05	0.03	0.01	2.49	7.16	0.08	0.23	0.01
Cm-CP2	1.83	8.00	0.08	0.10	0.01	2.81	7.08	0.05	0.04	0.01	2.49	7.15	0.09	0.23	0.01

[a] Cm-P and Cm-C are not stable structures in the gas phase.

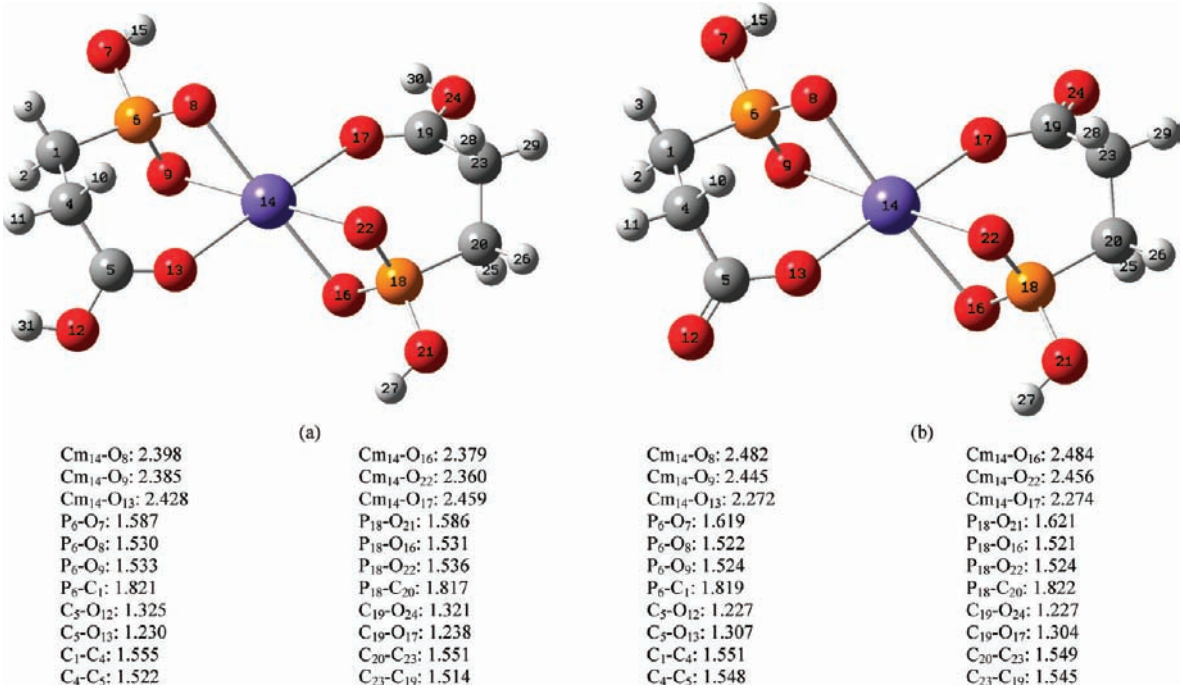

Figure 5. Optimized geometries (in Å) of (a) $Cm[H_2PPA]_2^+$ and (b) $Cm[HPPA]_2^-$ in aqueous solution.

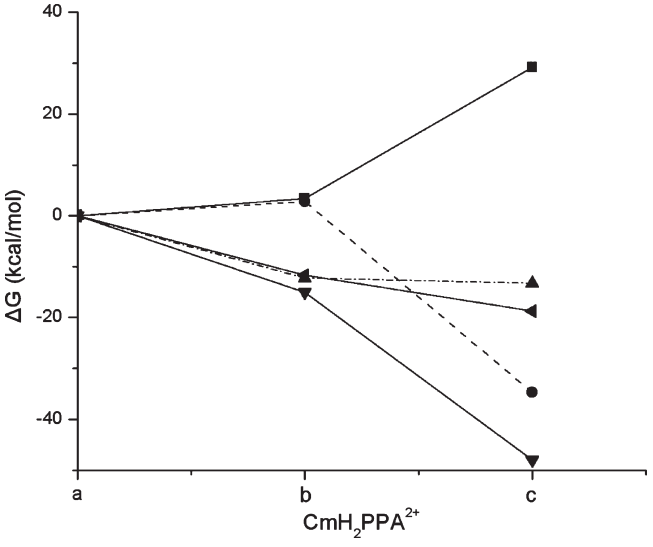

Figure 6. ΔE_g (solid square), $n\Delta G_{vap} + \Delta G_{clust}$ (solid circle), $\Delta G_{solv-clust}$ (up pointing solid triangle), ΔG_{solv} (down pointing solid triangle), and ΔG_{conf} (left pointing solid triangle) of (a) tridentate complex Cm-CP2, (b) bidentate complex Cm-CP, and (c) monodentate phosphate complex Cm-P of the CmH_2PPA^{2+} complex.

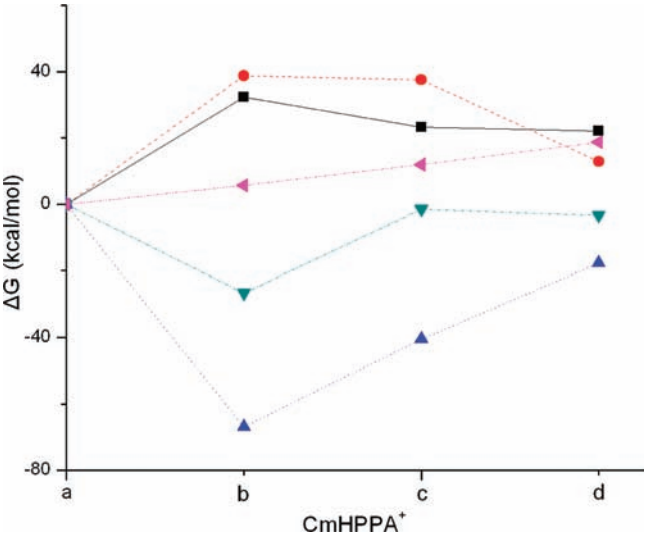

Figure 7. ΔE_g (solid square), $n\Delta G_{vap} + \Delta G_{clust}$ (solid circle), $\Delta G_{solv-clust}$ (up pointing solid triangle), ΔG_{solv} (down pointing solid triangle), and ΔG_{conf} (left pointing solid triangle) of (a) tridentate complex Cm-CP2, (b) bidentate carboxylate complex Cm-C2, (c) bidentate carboxylate complex Cm-P2, and (d) bidentate complex Cm-CP of the $CmHPPA^+$ complex.

($\Delta G_{solv-clust}$) and discrete contributions ($n\Delta G_{vap} + \Delta G_{clust}$) vary significantly from the tridentate complexes to monodentate phosphate complexes because of the changes in the numbers of water molecules in the first hydration shell around Cm^{3+}. The continuum contributions are also more sensitive to the level of chelation because the $HPPA^{2-}$ ligand carries an extra electron per ligand and is thus more sensitive to solvent influences. The variations in the contributions as a function of monodentate versus tridentate complexes is fully consistent with the fact that multidentate complexes displace more water molecules from the first hydration sphere.

3.4. Comparison with Observed Time Resolved Fluorescence Spectra. Fluorescence lifetime measurements can provide substantial insight into the composition of the first coordination sphere of Cm(III). Kimura and Choppin[8] have carried out fluorescence lifetime measurements of Cm(III) in aqueous solution by exciting to the F $^9I_{17/2,11/2}$ state of Cm(III) by a pulsed laser beam at 397 ± 1 nm and then monitoring the subsequent emission from the A $^6(D, P)_{7/2}$ state to the Z $^8S_{7/2}$ ground state. This transition occurs at 594−605 nm, which was measured by these authors to obtain the luminescence lifetime. .It is well-known that there is a linear correlation between the measured fluorescence decay constant (k_{obs}, the reciprocal of the excited-state lifetime) and the number of water molecules in the first coordination sphere of Cm(III)

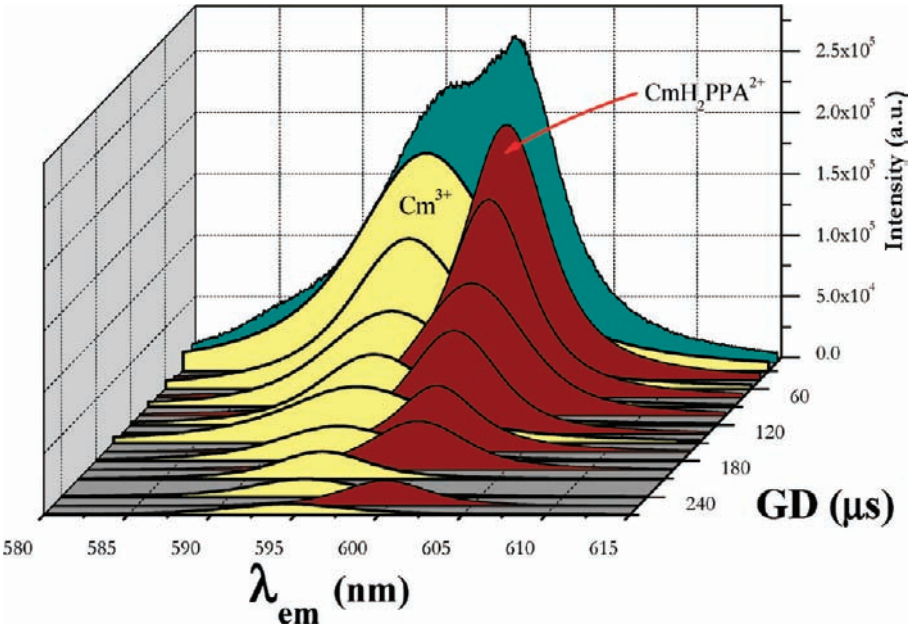

Figure 8. Deconvolution of the spectrum produces a signature for curium(III) and curium dihydrogen phosphonopropionate. $[Cm^{3+}]_{tot} = 6.8 \times 10^{-7}$; $[H_3PPA]_{tot} = 1.7 \times 10^{-7}$; pH 2.12. TRLFS Parameters: Shots: 1200/frame; GW: 500 μs; Slit Width: 500 μm; GD: 30 μs.

complexes, as shown by Kimura and Choppin.[8] These authors have derived the following empirical correlation relation for the fluorescence decay constants as a function of the hydration number in the first hydration sphere for Cm(III) aquo complexes:

$$n_{H2O} = 0.65k_{obs}(Cm) - 0.88r = 0.9938$$

where r is a correlation coefficient. If there is no contribution from the ligand to the de-excitation of the luminescent state, the hydration number of Cm(III) in different complexes can be obtained directly from the measured values of k_{obs} for a pure $[Cm(H_2O)_n]^{3+}$ complex. The measured lifetime of such a fully hydrated Cm(III) complex is 68 $\pm$ 3 μs. As water molecules are displaced from the first hydration sphere by other ligands, the fluorescence lifetimes increase, as the first coordination sphere is occupied by complexing ligands. The measured fluorescence lifetime of 68 μs for the Cm(III) aquo ion corresponds to nine water molecules in first coordination sphere in contrast to a value of 1300 μs when no water molecules are present in this sphere of Cm(III). Consequently, by measuring the fluorescence lifetimes of the chelated complex in solution, we could draw inferences on the nature of the complex and on how many water molecules would be displaced through the chelation process.

Figure 8 shows the deconvolution of the TRLFS obtained for Cm(III) complex with H_2PPA^-. The deconvoluted spectrum at pH 2.12 clearly shows evidence of a signature for curium(III) and the Cm-dihydrogen propionate complex. The TRLFS parameters for the spectra in Figure 8 are Shots: 1200/frame; GW: 500 μs; Slit Width: 500 μm; GD: 30 μs. On the basis of the evidence of formation of a complex of Cm(III) with H_2PPA^-, we have measured the fluorescence curium(III) complexed with phosphonopropionic acid at pH 4.47. Figure 9 shows the spectra together with the data fitted to four Voigt functions, shown as dashed lines. The peak maxima for free curium, curium dihydrogen phosphonopropionate, curium hydrogen phosphonopropionate are seen at 593.8, 599.5, 603.9, and 610.0 nm, respectively. The spectra shown for the hydrogen phoshonopropionate ion ($HPPA^{2-}$) support ring formation between curium and the phosphonopropionate ligand. The measured fluorescence lifetime of 160 $\pm$ 4 μs supports a displacement of five water molecules from the first hydration sphere, thus suggesting ring formation. Moreover the spectral peak corresponding to CmH_2PPA^{2+} increases in intensity as the total acid concentration is increased. The presence of an isosbestic point at 596.5 nm strongly supports the formation of a single complex at pH 2.1. Furthermore the validation plot for curium dihydrogen phosphonopropionate exhibits a slope of 0.83 $\pm$ 0.04 which provides further evidence of the formation of a 1:1 metal/ligand complex.

As we discussed in an earlier section, according to our calculations utilizing pure continuum IEFPCM model, the most stable complex for CmH_2PPA^{2+} in the aqueous phase is a monodentate complex with the Curium(III) bound to the deprotonated phosphate oxygen atom (Figure 2a). This conformation is consistent with our measured fluorescence lifetime of 72 μs for the 600.3 nm band of CmH_2PAA^{2+}, suggesting a displacement of one water molecule from the inner hydration sphere. Moreover, the fluorescence lifetime of the 599.3 nm band of CmH_2PPA^{2+} is even longer (112 μs), indicating a greater degree of displacement from the first hydration sphere. The lifetime for CmH_2PPA^{2+} indicates complexation with an additional oxygen atom on the phosphate group, but does not support ring formation. From the other geometries calculated, the next stable structure for CmH_2PPA^{2+} is a form of bidentate complex, where curium is part of a seven-membered ring with an oxygen atom from the phosphate and coordination with the carbonyl oxygen on the carboxylate group, as shown in Figure 2d. The energy difference between the two structures is only 7.09 kcal/mol, which indicates that it may represent a

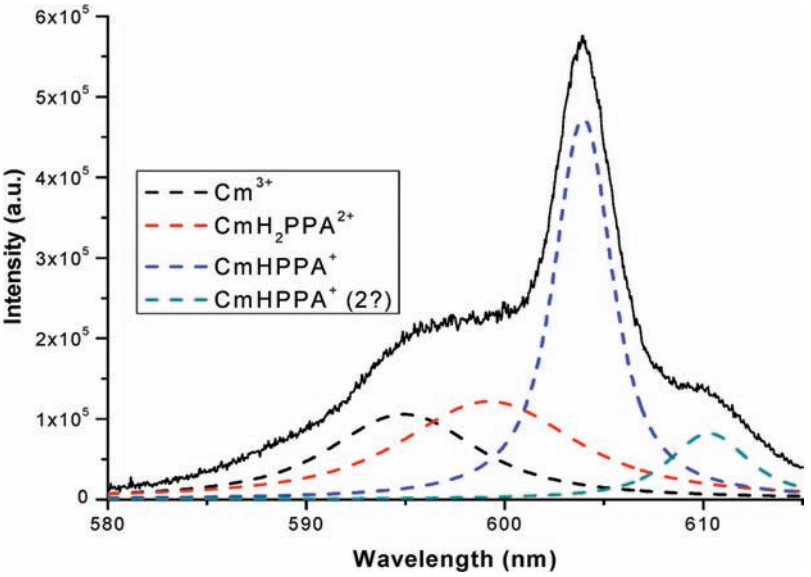

Figure 9. Fluorescence measurement for curium(III) complexed with phosphonopropionic acid at pH 4.47. $[Cm]_{tot} = 8.5 \times 10^{-7}$ M; $[H_3PPA]_{tot} = 1.2 \times 10^{-6}$ M. The data are fitted to four Voigt functions, shown as dashed lines. The peak maxima for free curium, curium dihydrogen phosphonopropionate, curium hydrogen phosphonopropionate are 593.8, 599.5, 603.9, and 610.0 nm, respectively. The respective full-width half-maximum values are 7.46, 8.86, 4.10, and 6.02 nm.

small component among a mixture of species that exist in solution. This structure should represent a larger increase in fluorescence lifetime from the free ion than what is observed in the fluorescence data of either complex.

There are three structures in the aqueous phase that are considered to be the most stable by our calculations, shown in Figure 3 (3a, 3d, 3f). Among these structures, the most stable complex determined for $CmHPPA^+$ in the aqueous phase is a seven membered ring, shown in Figure 3f. In this structure, the curium is bound to two phosphate oxygen atoms and one carboxylate oxygen atom of the same $HPPA^{2-}$ ligand. The ring presented in Figure 3f has the capability to displace a larger number of water molecules than the carboxylate coordination shown in Figure 3d or the monodentate phosphate coordination shown in Figure 3a. This structure in Figure 3f supports the fluorescence lifetime observed for the $CmHPPA^+$ complex (172 μs), which indicates the removal of as many as six water molecules from the inner hydration sphere. The full-width at half-maximum value of this emission is about 4 or 5 nm, which is significantly less than for the emission of a free curium ion (fwhm = 8 nm). The sharp nature of this fluorescence peak can also be found for the curium dihydrogen ethylenediamine tetraacetate complex, CmH_2EDTA^+, which strongly suggests ring formation.

Furthermore, fluorescence lifetime measurements determine a similar change for the analogous complex with phosphonoacetic acid, $CmHPAA^+$, which is composed of three additional water molecules in the first hydration sphere displaced from CmH_2PAA^{2+}. While this additional displacement indicates a higher degree of complex, it is still less than what is observed for the longer-lived $CmHPPA^+$complex . The $CmHPAA^+$ complex exhibits a fluorescence lifetime value between that of a monodentate interaction and the formation of the six-membered ring. The carboxylate coordinated structure in Figure 3d is supported by the fluorescence lifetime data for neither the phosphonoacetic ($CmHPAA^+$) nor the phosphonopropionic acid ($CmHPPA^+$) complex.

The carboxylate group effectively competes with the phosphate group for Cm(III) in aqueous solution, that is, Cm-CP is even more unstable for $CmHPPA^+$. The most stable structure is the tridentate complex Cm-CP2. This might explain why the lifetime of $CmHPPA^+$ is 160 μs while the lifetime of CmH_2PPA^{2+} is 112 μs. Thus, $CmHPPA^+$ exhibits fewer coordinated water molecules in the first hydration sphere than CmH_2PPA^{2+} in the solution, primarily because of an increased water displacement by the ligands for $CmHPPA^+$.

4. Conclusions

Extensive computational studies on Cm(III) complexes with the PPA ligand reveal the existence of several possible low-lying structures in aqueous solution and dramatically different structures in the solution phase compared to the gas phase. We have studied different structures arising from CmH_2PPA^{2+}, $CmHPPA^+$, $Cm[H_2PPA]_2^+$, and $Cm[HPPA]_2$ which have revealed many ways the PPA ligands can bind to Cm(III). The TRLFS measurements of these complexes in solution as a function of pH provided valuable information on the nature of these complexes and the number of water molecules present in the first coordination sphere. Our computations showed that the solvation effects are critical to the determination of the preferred configurations and binding propensities of carboxylate versus phosphate groups. Our computed structures of the complexes in solution and free energies of solvation facilitated the interpretation of the experimentally observed fluorescence spectra and the lifetimes of these complexes. It has been observed that as more water molecules are displaced from the first hydration sphere by the ligands that bind to Cm(III), the fluorescence lifetime increases.

Our computations show that the most stable complex for CmH_2PPA^{2+} in the aqueous phase is labeled Cm-P, a monodentate complex where the curium(III) is bound to

the deprotonated phosphate oxygen atom. This structure is consistent with our measured fluorescence lifetime of 72 μs for the 600.3 nm band of CmH_2PAA^{2+}, suggesting a displacement of one water molecule from the inner hydration sphere. On the other hand, the fluorescence lifetime of the 599.3 nm band of CmH_2PPA^{2+} is even longer (112 μs), indicating a greater degree of displacement from the first hydration sphere suggesting the possibility of a mixture of low-lying isomers in the solution. This lifetime for CmH_2PPA^{2+} indicates complexation with an additional oxygen atom on the phosphate group, but does not support ring formation.

For the Cm-$HPPA^+$ complex we have found three low-lying structures in the aqueous phase that are shown in Figures 3a, 3d, and 3f. Among these structures, the most stable complex determined for $CmHPPA^+$ in the aqueous phase is in Figure 3f, which exhibits a seven membered ring. The stable tridentate form for $CmHPPA^+$ structure supports the observed fluorescence lifetime for this complex (172 μs), confirming the removal of up to six water molecules from the inner hydration sphere.

Complexation for the curium(III)-PPA system above a pH 6.5 has not been extensively studied by TRLFS. As the solution pH is increased above 7.00, the second deprotonation of the phosphate group should produce a more stable interaction between Cm(III) and the phosphate group of the phosphonopropionate ion in the seven membered ring complex, CmPPA. This structure may exhibit similar fluorescence properties to the $CmHPPA^+$ structure shown in Figure 3f.

The relative stabilities of the complexes are found to vary substantially between the gas phase and solution, indicating a major role of the solvation in the relative stabilities of these complexes.

Acknowledgment. This research was supported by the U.S. Department of Energy under Grant DE-FG02-05ER15657. The work at LLNL was performed under the auspices of the U.S. Department of Energy. The authors would like to acknowledge computational support on Lawrence Livermore's supercomputer comprising 992 processors supported by DOE's accelerated supercomputing initiative program. M.G.C. was supported by a Department of Energy, Office of Civilian Radioactive Waste Management Fellowship.